Kurdish Studies
September 2024
Volume: 12, No: 5, pp 1978-1989
ISSN: 2051-4883 (Print) | ISSN 2051-4891 (Online)
www.KurdishStudies.net

DOI: 10.53555/ks.v12i5.3968

Seismic Risk Analysis And Crustal Thickness Identification With Prospective Destruction To Infrastructure In Gilgit City And Surrounding Areas, Pakistan

Adil Naseer[a*], Tahseenullah Khan[b], Nasir Mehmood[c]

[a*,b]Department of Earth and Environmental Sciences, Bahria University, Islamabad 44000, Pakistan
[c]Seismic Monitoring Centre, Pakistan Meteorological Department, Islamabad,44000, Pakistan

***Correspondence:** Adil Naseer
*Email: adilnaseer_bu@yahoo.com

Abstract
Pakistan is a country that holds a key position in South Asia due to its regional topography. Gilgit experiences frequent earthquakes due to its tectonic position between the Indian and Asian continental plates. Two major seismic zones; Main Karakoram Thrust (MKT) and Main Mantle Thrust (MMT) have been identified to create great seismic activity in the surroundings of Gilgit City. It is important to understand the seismicity patterns of earthquakes in Gilgit city based on their source mechanism. The key objective of the research was to assess the causes of Earthquakes and predict the possibility of forthcoming earthquakes. The waveform data was utilized and for the first time, deeper crustal structure was determined successfully. Seismological data was used to evaluate the crustal thickness and structure of the S-wave velocity underneath the Gilgit area. Primary wave receiver function (PRF) analysis, H-K stacking and inversion techniques were applied for this purpose. A new crustal model for S-wave velocity with maximum crustal thickness was identified. H-K stacking technique occurred to the receiver functions representing estimating the width of crust (H) and Poison ratio (K). The reasonable stable and high horizontal velocity and phase of a teleseismic P-wave were identified. The GSAC tool and the Computer Programmed in Seismology CPS.330 were used to obtain seismograms of earthquake events in the past two years. Also, the SALENA risk tool was utilized for the estimation of loss and damage considering the worst-case scenario for the Earthquake (Mw 7.0) along the MMT zone of Gilgit City.

Keywords: Gilgit City, earthquake, waveform, Moho discontinuity, teleseismic

1.Introduction

Pakistan is a country that holds a key position in South Asia due to its regional topography including mountains in the North, South and west, with plains in central Punjab, Sindh and coastline in the Arabian Sea in the South (Rehman and Burton, 2020). The country has a dense seismic environment and holds a 44th position out of 50 countries with global seismic hazards (Tsapanos and Burton, 1991). The high density of active faults in north Pakistan makes it seismically the most important active zone in the area (Khalid et al., 2016). Northern Pakistan is categorised into four main divisions: Karakoram, Hindukush, Turan, and Kohistan (Qureshi et al., 2021). Gilgit is the capital city of Gilgit-Baltistan (GB) province in the Himalayan region between 35–37°N latitudes and 73–75°E longitudes. The tectonic setting of this region is because of the tectonic accretion of the Indian continental plate with the Asian continental plate in the Eocene (Searle and Treloar, 2019).

Gilgit experiences frequent earthquakes due to its tectonic position between the Indian and Asian continental plates (Qureshi et al., 2021). Two major seismic zones i.e. Main Karakoram Thrust (MKT) and Main Mantle Thrust (MMT) have been identified to create great seismic activity in the surroundings of Gilgit city that can impact not only Gilgit but other regions of Northern Pakistan (Waseem et al., 2018). According to Pakistan's Building Regulations (MoHW, 2007) and probabilistic seismic hazard assessment for northern Pakistan, Gilgit City lies in Seismic zone II with the maximum possible ground motion range between 0.25-0.4g that correspond to intensity level VI-VII on the MMI scale (Rahman et al., 2021; Waseem et al., 2018). The seismotectonic map around Gilgit indicates shallow earthquakes are frequent in and around the Himalayan seismic zone while intermediate-depth earthquakes are mostly generated from the Hindukush Region (Figure S1, supplementary material). Due to economic constraints, and poorly constructed buildings, the city experiences a significant amount of damage. Recently occurred earthquakes along the MMT-Raikot fault i.e. Astore 2002 (Mw 6.3), 2019 (Mw 5.6), 2021 (Mw 5.3) and MKT fault earthquake 2012 (Mw 5.6), have resulted in a strong shaking effect and damages near Astore and Gilgit city. Any strong earthquake in future could affect Gilgit city with serious risks to infrastructure and life. Unfortunately, no significant studies were performed based on seismic risk assessment using the latest risk computational tools, although the town has faced many strong earthquakes in history due to its presence close to the active seismic zones (Ahmed et al., 2021). These facts highlight the importance of efficient seismic monitoring for such an active seismic zone along with considerable efforts for revised seismic hazard evaluation and effective risk measurement to mitigate the level of risk with appropriate solutions.

The major aim of the research was to understand seismicity patterns among source mechanisms of earthquakes that occurred in and around Gilgit City. One of the major objectives is to find out the seismic activity of Gilgit City and adjacent areas using the waveform data of the PAKISTAN SEISMIC CENTER seismic network, for achieving consideration of the causes of earthquakes and assessing the possibility of forthcoming damaging earthquakes and optimizing the information in terms of

detail seismicity pattern. Due to the unavailability of a dense seismic monitoring system to our knowledge, no study has been reported for determining the deeper crustal structure. This study is a novel approach for determining the crustal thickness through broadband seismic waveform data from broadband seismic stations installed in Gilgit City.

2. Materials and Methods

a. Major Seismological Analysis Techniques and Seismic Risk Assessment

Seismological analyses were carried out under this study involving receiver function analysis, local earthquake analysis for hypocenter location and moment tensor inversion for source mechanism estimate for the Gilgit area.

b. Crustal Structure and Local Earthquake Analysis

The crustal structure is estimated for the study area using seismic waveform data of the local broadband seismic station installed at Gilgit. The phase arrival data from the seismic network is analysed with various techniques to locate hypocentres and determine the intensity of earthquakes. The duration of local and regional records may range from seconds to a few minutes. The frequency of these events is high in the order of frequency > 1 Hz and they are recorded well both on short-period and broad-band instruments. Normally a sampling rate of 100 Hz is applied for local stations for such events (Qadri et al., 2023). It is possible to determine earthquake hypocentre locations, magnitude estimate, focal mechanisms, upper portion of mantle and crust structure using seismic waveform records from a single station or local seismic network by picking P and S-waves recording times correctly and other later phases for determining amplitudes from the observed seismic waveform records (Ahmed et al., 2023).

c. Seismic Waves of Local Earthquakes

In the local seismic network of the PAKISTAN SEISMIC CENTER including both short-period and broadband seismic stations, it is observed average seismic station spacing local seismic network may range from 50 km to 300 km (Zahoor et al., 2023).

"Capacity Spectrum Methods (CSM)" or analytical methods which provide a volume curve (Wilson et al., 2008). The technique is based on the steps including i) Transformation of capacity curve into SA–SD domain ii) Assigning damage state thresholds and standard deviations iii) Construction of fragility functions for each damage state ds iv) Overlaying capacity curve with demand spectrum v) Identification of Performance point by iterative procedure vi) Assigning of discrete damage probabilities by the multiplication of available numbers of buildings with discrete damage probabilities in a certain area i.e. geo unit, for which the absolute damage extent is estimated.

d. Seismic Risk Assessment Tools

The SELENA Risk Assessment tool was used as a seismic risk assessment tool (Molina et al. 2010). SELENA. HAZUS–MH not only provides the core procedure but is also considered an independent risk assessment tool that uses capacity-spectrum methodology with flexibility in basic datasets and input parameters. It also has a GUI interface of MATLAB code and it can be adapted into any specific study which is further integrated within a logic-tree computation system. It has a capacity that takes epistemic uncertainties in input parameters and models (Poudel et al., 2023).

e. Statistical Analysis

In this study, various seismological and mapping tools are used including:

1. GSAC and SAC software for Seismic waveform Data Processing
2. Computer Programs in Seismology PROGRAM. 330 developed by R.B. Herman (Latest tools modified 2022 for Ubuntu 20.04 for Receiver Function Computation)
3. SEISAN 11.0 for Hypocenter Location
4. Taup-Toolkit for theoretical travel time estimate travel.
5. Geopsy for H/V computation
6. Google Earth and ArcGIS 10.6 map programs are used to make polygons for geo units and demarcation of the study area.
7. MATLAB Tools is used to compute damage results, and human and economic loss in this study.
8. Generic Mapping Tool (GMT 6.4) is utilized for charting SELENA output results, seismicity catalogue and source mechanisms.

3. Results and Discussion

a. Crustal Structure Determination near Gilgit

Teleseismic P-wave receiver function analysis for crustal arrangement determination underneath the broadband seismic position GLGT (Gilgit) located in Higher Himalayas (North Pakistan) has been carried out. The research area is Gilgit city in the Higher Himalayas, which is dominated by complex tectonic features with active thrusting and deformation processes. Present research, time-domain receiver function analysis is used in a stage-wise approach; from authentic three-component waveform data to determine crustal structure and velocity of secondary wave estimate for GLGT seismic stations. Fig. 1 shows a simple ray path for the incident primary wave, PS converted and different reverberation from the interface. The horizontal velocity and phase of a teleseismic subsurface wave (P-wave), which reaches the seismic location, is reasonably stable and high (15–25 km/s). This velocity and phase value supports a planer wave and makes it easier to analyze the ensuing movement of the ground. (Melouk et al., 2023).

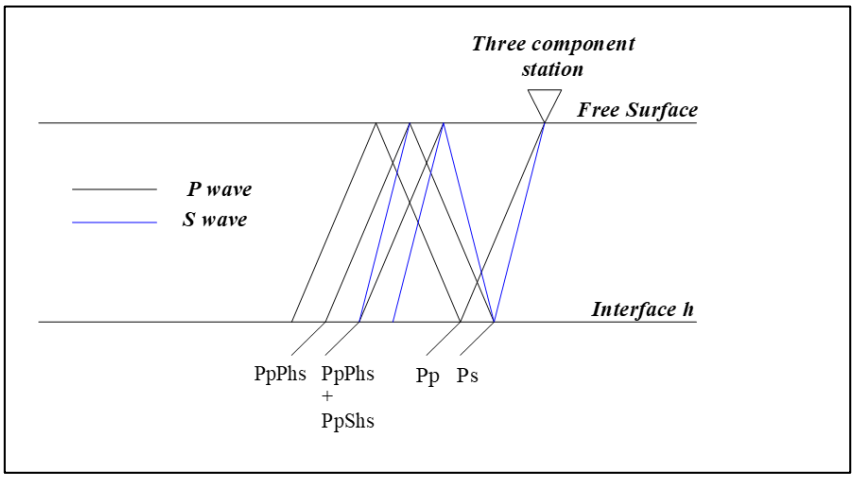

Fig.1. A straightforward ray diagram illustrating the phase of the Moho reflecting primary to secondary wave conversion, which comprises the receiver function for just one layer spanning a half-space underneath the seismic record station.

Seismic Data Processing for Receiver Function Analysis

The criteria for the choice of earthquakes applied in the receiver function analysis are based on Strong magnitude earthquakes i.e. Mw > 6.0 was selected as having good signal strength, with well clear P-wave onset. Selection of teleseismic earthquake data from the USGS earthquake catalogue considering the reliability of their global hypocenter locations and magnitude estimates. Teleseismic events with an epicentral range of 30° - 90° are selected, as the seismic waves travelling in this distance range when reaching the seismic station, these waves propagate over the crust and mantle, developing in Moho reflected P to S transformations (Nemocón et al., 2021). Such signals are used further in the receiver function method. Therefore, teleseismic waves for P-waves invented from earthquakes at an outward gap farther than 30° carry information about the earth's structure (Li and Mashele, 2009).

Identification of Earthquake with Good Signal-to-Noise Ratio (SNR)

Fig. 2 presents the occurrence of 58 seismic events from 2019 to 2022 that occurred at the GLGT seismic station for the RF (Receiver Function) study. The SAC tool was used to execute a quick and dirty visual filtering procedure to find and eliminate unwanted events. The seismograms for the incidents (58 occurrences from 2019-2022) were extracted and displayed using the GSAC tool and the Computer Programmed in Seismology CPS.330.

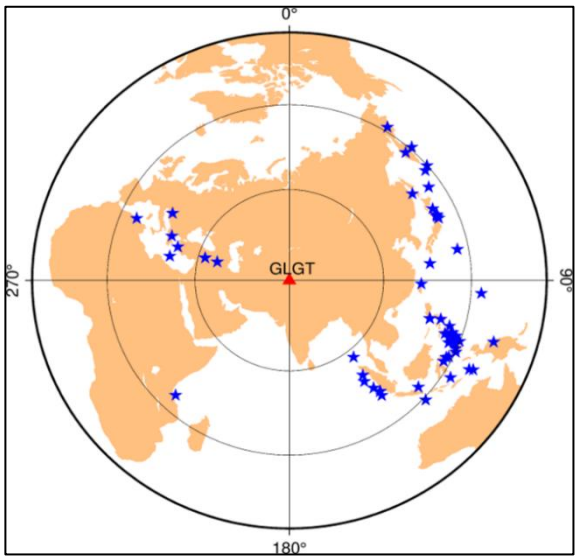

Fig.2. Showing the location of GLGT station and global division of teleseismic results applied for receiver function calculation.

Occasions with magnitudes of moments greater than Mw > 6.0 that occur at epicentral intervals between 30° and 90° from GLGT place were chosen for this process. The amount of distortion and the clarity of the straight P-wave appearance on the seismograms is a useful method to gauge the events' intensity (Melouk et al., 2023). Studies prove that many events in this region come from the West, primarily from Greece and Turkey, either produced a lot of noise or made it impossible to distinguish wave arrivals (Goldstein et al., 2003).

Rotation of Horizontal Channels

Fig. 3 shows the Horizontal channels HHE and HHN for the above Taiwan earthquake recorded at GLGT stations rotated into HHR (radial) and HHT (tangential) components. The original waveform was converted from ZNE to ZRT format. The transverse component is perpendicular to the radial component, which emanates from the event and points in the direction of the station. When it comes to waveform isolation, one method considers that body waves (P-waves) have a near-vertical incidence and are contained in the vertical component of the waveform whereas the resulting S-waves are included in the radial component. The incident waves caused by to change in incidence angles may result in some signal leakage between the components (Buchan et al., 2023). This assumption is standard to the initial sequence and has been used in teleseismic receiver function research (Li and Mashele, 2009).

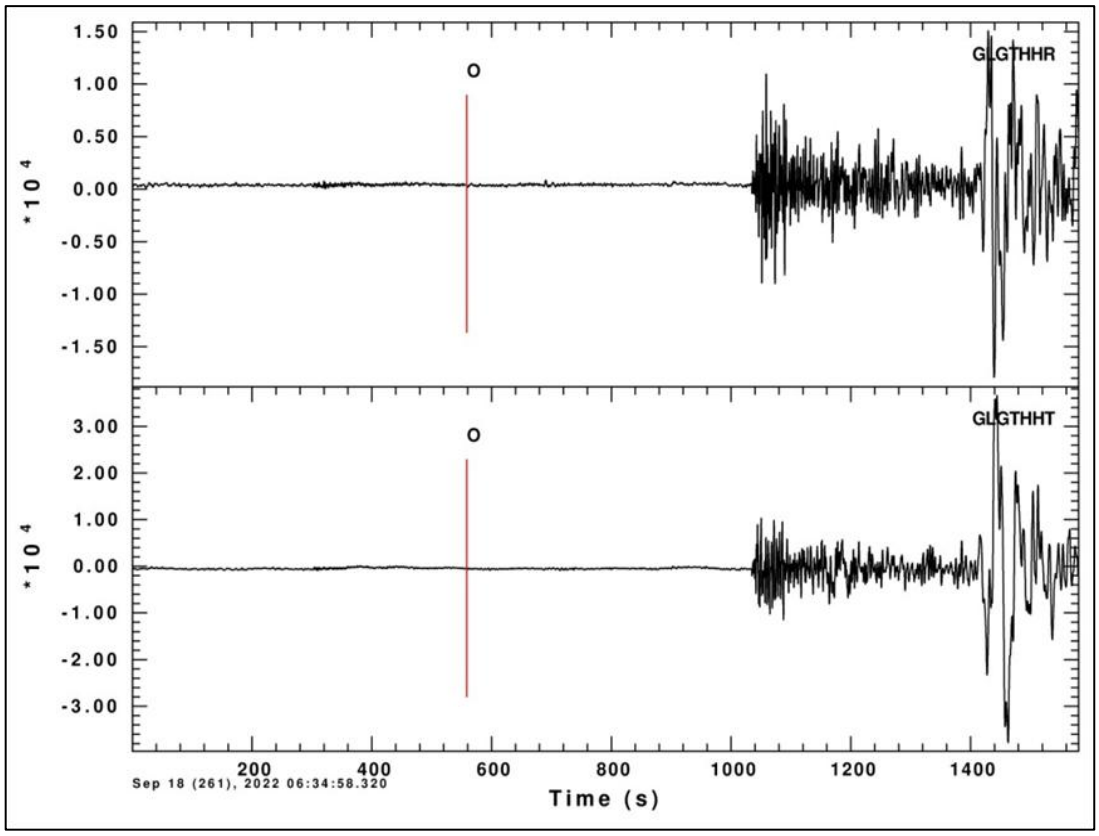

Fig.3. Horizontal channels HHE and HHN for the above Taiwan earthquake recorded at GLGT rotated into HHR (radial) and HHT (tangential) components.

The coordinate system LQT was used to isolate the waveform energies, and an all-three-element system spun in the form of ZRT components in the polarization orientation of the resulting primary wave (Torsvik, 2015). This coordinate system is used to isolate the receiver response that needs the ZRT system. To orient the element along the angle provided by the station to the event back azimuth (plus or minus 180 degrees), linear data was rotated during this operation. The two horizontal elements rotated into the radial (R) and tangential (T) components when rotation is applied, leaving the vertical component (Z) unchanged (Wessel et al., 2013).

Receiver Function for GLGT

Since the Earth's structure is not uniform, every seismic activity has a unique pattern as it moves from the epicentre to the reception location. To demonstrate such distinctiveness, receiver function approximations for a couple of stations were obtained from the GLGT stations and were contrasted in Fig. 4. They are sorted into both back-azimuth (BAZ) and Ray-parameter p (s/km). There are a few variations in the receiver functions, but overall, they are fairly comparable. Therefore, the non-uniformity in the Earth structure, allows every seismic activity to own a unique pattern as it moves from the epicenter to the reception location. As a result, every receiver function prediction produced by deconvolution will give different results (Wang et al., 2016).

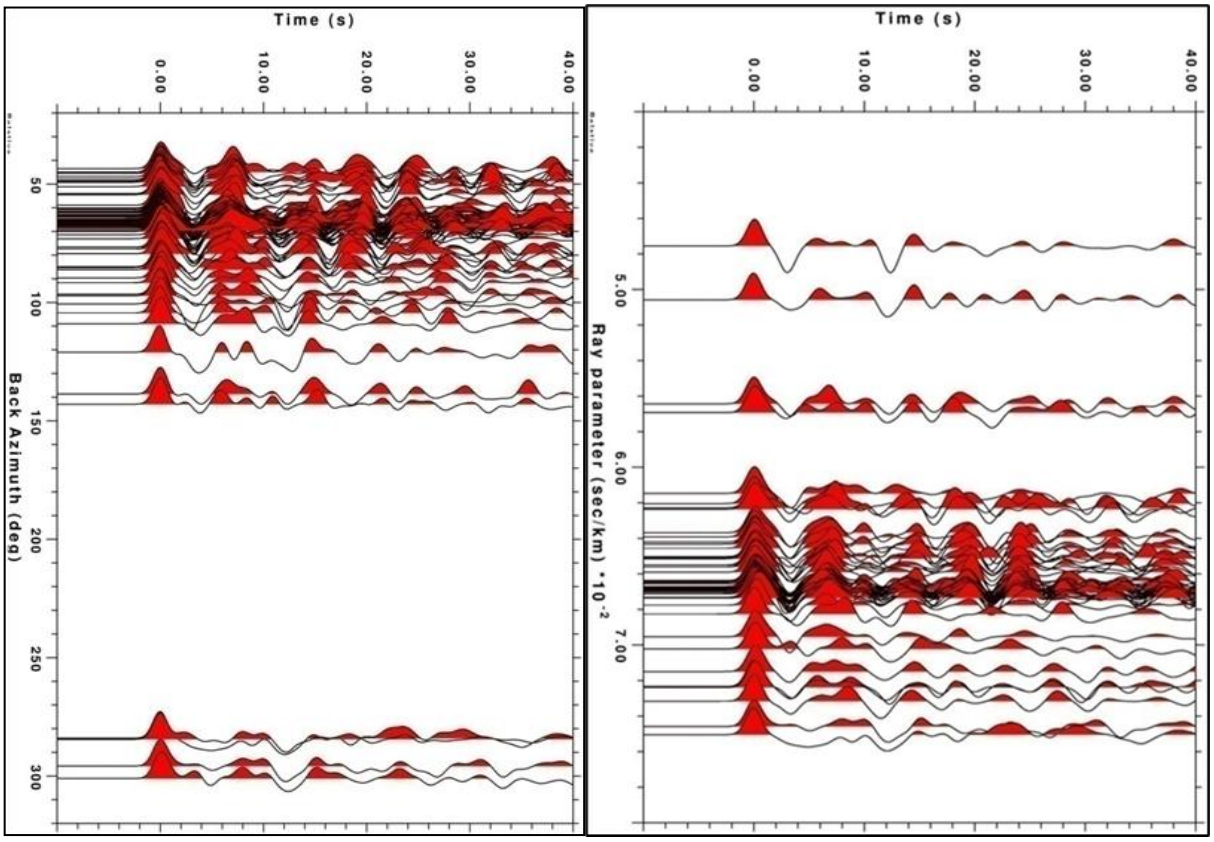

Fig.4. Output of the RF-stacking shown for Radial receiver functions, stacked corresponding back azimuth, BAZ (left) and ray-parameter, p (s/km) at alpha 1.0 Hz for GLGT station.

Fig. 5 (a) presents plots of R-F Stacking for the Radial receiver function estimated beneath GLGT stations at Gaussian filter Alpha 1.0 Hz. The Moho's transformed phase P to S, also shown by the thin line (cyan coloured) stacked according to the BAZ range has been mentioned. The bull's eye plot was received (Fig. 5b) using the Matlab tools described by Zandt and Ammon (1995). The plot is called a move-out plot is a stack of all of the receiver functions from the station migrated to depth using a fixed Vp of 6.4 km/s and the Vp/Vs ratio calculated using the HK stack.

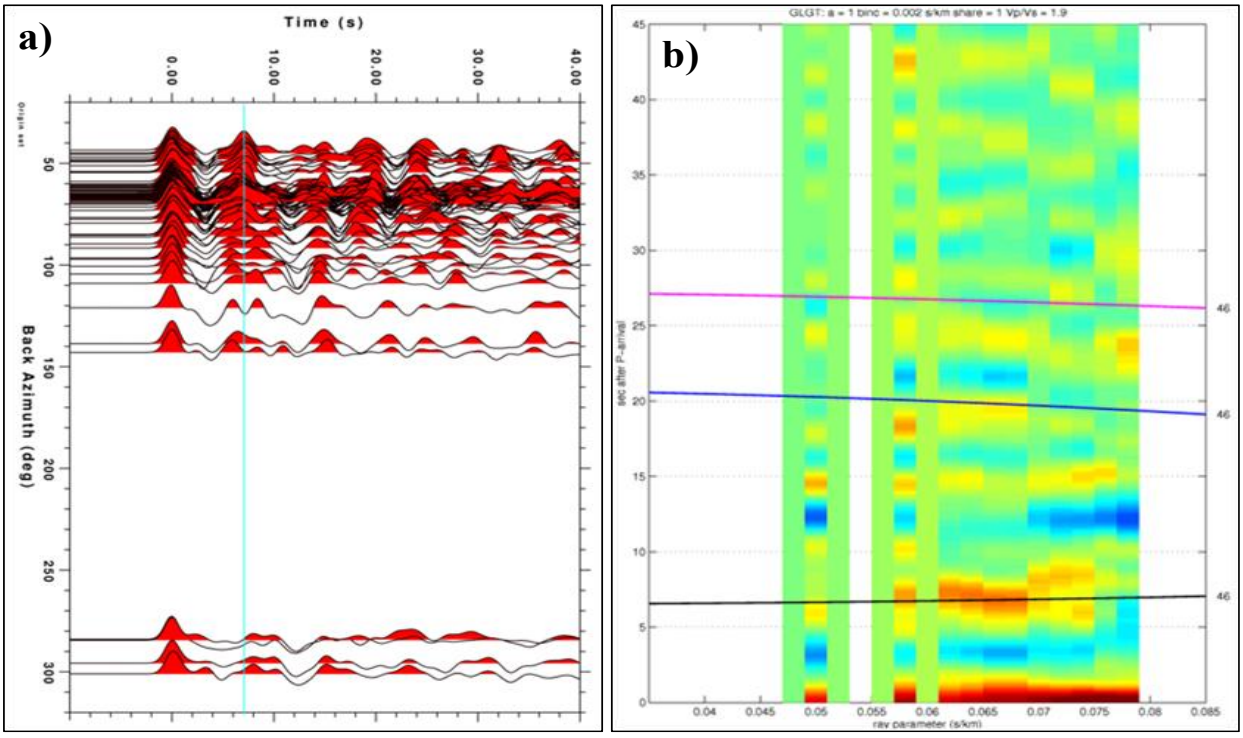

Fig.5. (a) Results of the RF-stacking shown for Radial receiver functions for GLGT station at alpha 1.0 Hz. Moho converted the PS phase shown by a thin line (cyan-coloured line) stacked according to BAZ. **(b)** Radial receiver function phasing diagram for GLGT stations with receiver functions binned using slowness and plotted as a function of slowness.

The plot helps determine if an arrival is a primary or a multiple. Primary arrivals (the black line) have a positive slope while multiples have a negative slope (blue and red). The location of the lines is based on the results of the HK Bulls' eye.
Every receiver function is categorized into bins created on slow nesses and graphed as a function of slowness. Duskier shading is cast off to denote positive amplitudes, while lighter shading shows negative amplitudes. By viewing the changes in arrival time for numerous phases as slowness increases, the occurrence of Moho and other discontinuities can be readily detected. The theoretical arrival times are calculated using a one-dimensional model. Ray parameter versus time after P wave. The entire Pds ray set is binned by ray parameter and mean traces are formed for each bin. Plotting all these summary traces together forms the above image. Black and white shading represents ± 0.05% amplitude of the radial P wave. The move-out curves for the indicated discontinuity depths have been plotted. Moho and other discontinuity-reflected phases are clearly shown in the plot. The 2p1s Moho reverberation arrives at 7-9 seconds, and the energy between this time series is the combination of energy reverberated from lithosphere discontinuities with direct Pds.

Moho Thickness and Vp/Vs

The H-k stacking method, developed by Zhu and Kanamori in 2000, has been utilized to determine the crustal thickness (H) and Vp/Vs ratio (k) for the GLGT stations. A simplified model for H-k and VpVs based on the above technique is denoted in Fig. 6. The determinations of crustal thickness, average primary velocity, and Poisson's ratio derived from seismic waves serve as valuable constraints for understanding the overall composition and evolutionary models of the Earth's crust (Melouk et al., 2023). The transformed phase angle Ps and Moho multiples (2p1s, 2P2s, etc.), specific in teleseismic receiver functions, have been employed to ascertain the crustal thickness (H), Vp/Vs ratio (k), and Poisson's ratio (s).
This technique involves employing a stacking algorithm that utilizes both the directly arriving P-to-S conversion (PS) and the subsequent multiples resulting from crustal reverberations (multiples) such as PpPs and PpPs+PpSs. The primary objective of this method was to estimate the crustal thickness (H) and the average Vp/Vs ratio (ϰ) by analyzing the receiver function time series (Zhu and Kanamori, 2000). The Vp/Vs ratio is closely connected to the Poisson ratio (σ), which is known to offer improved insights into crustal composition when analyzing P- or S-wave data in isolation (Kraft et al., 2019; Wang et al., 2016; Wen et al., 2019). The technique utilizes the time delays of Ps, PpPs, and PpSs+PsSs to convert the receiver function from the time domain into the H-k stacking domain. The most accurate estimation of crustal thickness and Vp/Vs ratio is achieved when the three phases undergo stacking and exhibit the highest level of coherence (Wen et al., 2019; Zhang and Huang, 2019).

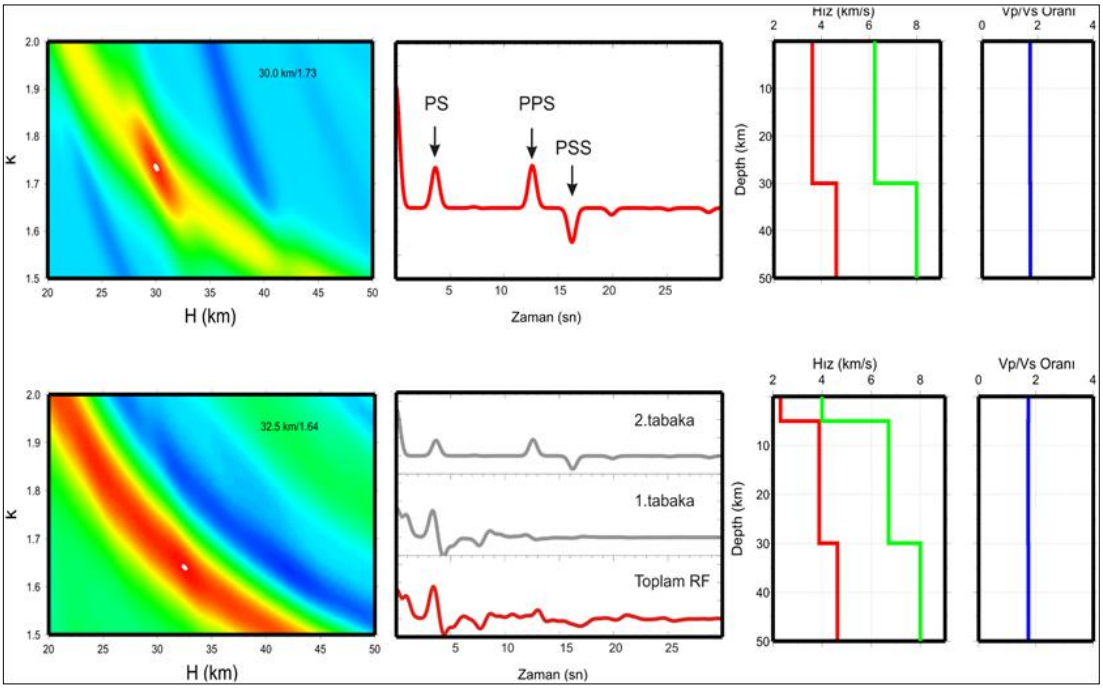

Fig.6. Simplified RF Moho PS conversion and Hk-Stacking pattern shown in the plot.

However, the H-k stacking approach is quite helpful even for a single-layered average crustal model. However, the Moho depth and velocity contrast appear when the mean crustal primary wave rate is altered (Ammon et al., 1990). The receiver function obtained in this study provides two important parameters that describe the structure of the crust. The mean crustal Vp/Vs proportion, which is only connected to the elasticity nature of the crust, and the Moho depth serve as indicators of the thickness of the crust. Poisson's ratio is expressed by:

$$\sigma = \frac{\left[\left(\frac{Vp}{Vs}\right)^2 - 2\right]}{2\left[\left(\frac{Vp}{Vs}\right)^2 - 1\right]} \qquad (1)$$

In the above equation σ Poisson's ratio was determined using the above equation (1) for GLGT stations. The influence of lateral variations is mitigated by stacking computed receiver functions acquired from diverse ray parameters and back azimuths. In the H-k stacking method, a mean crustal P-wave velocity of 6.4 km/s was assumed, and weighting parameters of 0.7 were assigned to Ps arrivals and 0.2 to PsPs multiples. In a typical receiver function study, the range of slowness employed does not seem extensive enough to eliminate the ambiguity between depth and velocity. Therefore, the incorporation of a priori information becomes essential (Torsvik, 2015).

Fig.7. represent the results for the GLGT Receiver function calculated by deconvolving vertical RF from radial components of ground motion. The waveform data was examined to process receiver functions and remove those with noisy or low SNR (signal-to-noise ratio).

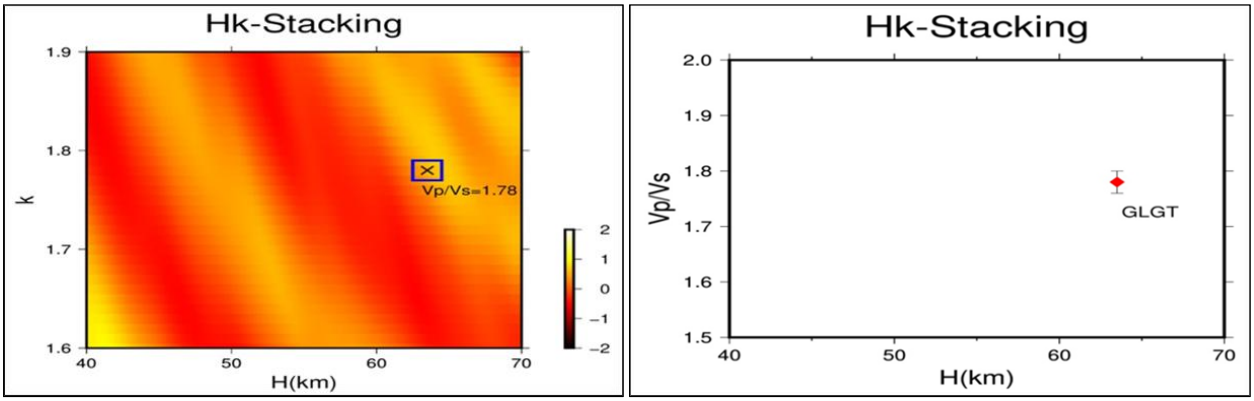

Fig.7. The vertical component of ground motion was separated from the radial components to yield receiver functions.

Waveform data was carefully examined before processing the receiver functions, and any receiver functions with a low signal-to-noise ratio or considerable noise was disregarded. Thus, about 58 radial receiver functions were left behind for more study. To begin with, the S-wave velocity was calculated using the one-dimensional tectonic velocity model offered by crust 2.0 and a Vp/Vs ratio of 1.74.

The single station H-k stacking approach, which offered useful constraints, was used to establish the crustal thickness and bulk crustal Vp/Vs ratio in the northern region of Pakistan. The crustal thicknesses and Vp/Vs ratios of 56-63.5 km and 1.74-1.84 were found, respectively. According to the initial findings, there may be a Moho below the stations. Previous gravity studies found a 32–35-kilometre solid crust in our research area (Aslam et al., 2021; Khurram et al., 2021). The metamorphic crust corresponds with Poisson's ratios of 0.26 to 0.29. The 1-D velocity arrangement estimated underneath a broad-band station is represented in Table S1 (supplementary material).

The Fig.8 (a) displays the earth model once more, along with the corresponding receiver functions. S-wave velocity structure estimated beneath GLGT station and AK135 reference model was used with an indication of Moho at GLGT. Inversion of P wave radial RF results indicate a shear wave velocity of 3.62 km/s in the crust of Gilgit station located in the Higher Himalayas thrusting region to 4.5km/s underneath the Moho limit.

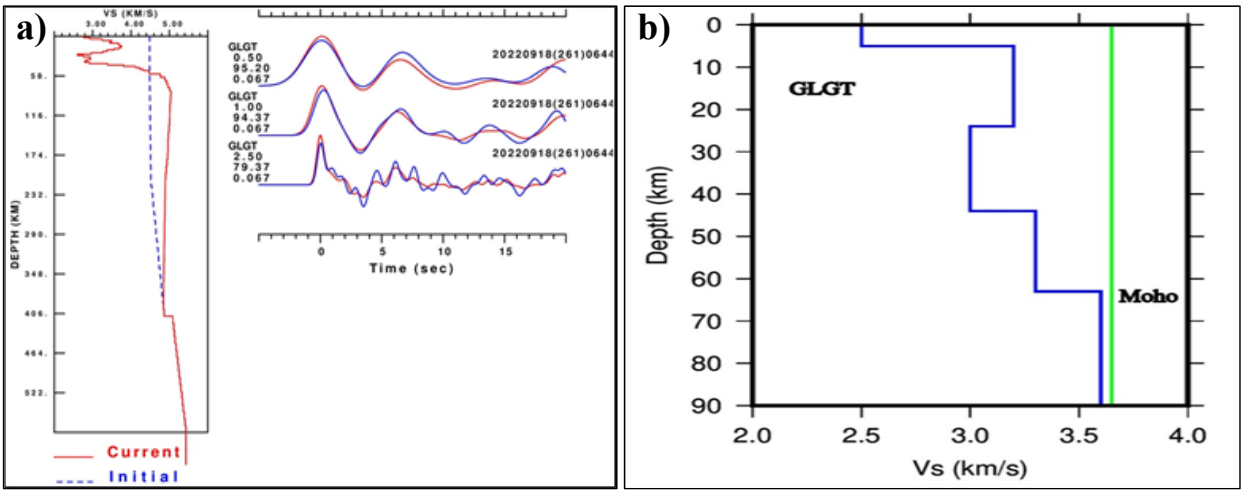

Fig.8. (a) Inversion of Receiver Functions for Gaussian Filter parameters at 0.5 Hz, 1.0 Hz and 2.5 Hz **(b)** Resulting in one-dimensional S-wave velocity for GLGT stations.

The Moho depth achieved underneath the GLGT station is around 63.5 km in northern Pakistan with a typical Vp/Vs ratio ranging from 1.74. The occurrence of a sedimentary rock layer at a depth of around 15 km, which results in a 2-second lag in the earthquake signal, is mostly to blame for the presence of the complicated character of the crust as shown by the Moho-

converted PS phase, beneath the station GLGT. Radial receiver functions show a clear strong signal between 7 to 9 seconds, which is interpreted as a conversion from the Moho boundary.

Using the AK1 and IASP91 velocity models, the receiver functions (RFs) were back-projected and stacked across the appropriate ray paths. To further study the peculiarities of the crust, the SRTM topography was plotted. Within the research area, differences in both the lower and upper crust's structure were seen beneath the surface. At a depth of 56–64 km, a visible Moho discontinuity was photographed below the GLGT stations. The Moho conversion in Pakistan's northern region showed a low amplitude, with a greater amplitude transformation taking place at depths of 50–60 km (Eulenfeld, 2020). The existence of anisotropy crust and the impact of descending layers, that show fluctuations from south to north, are indicated by considerable transverse energy with huge amplitudes. Under the middle crustal block, these impacts are extremely strong.

A significant spike in a duration of 7-9 seconds, notably at the GLGT station, is also seen, as well as a crustal conversion that happens about 2-3 seconds after the P-arrival. For the station shown in Fig.8. (b). It has been noted that a model with greater complexity beyond a single-velocity crust is needed to comprehend the phenomena. The findings demonstrate that the S-wave velocity underneath northern Pakistan rises between 3.6 km/s to 3.8 km/s.

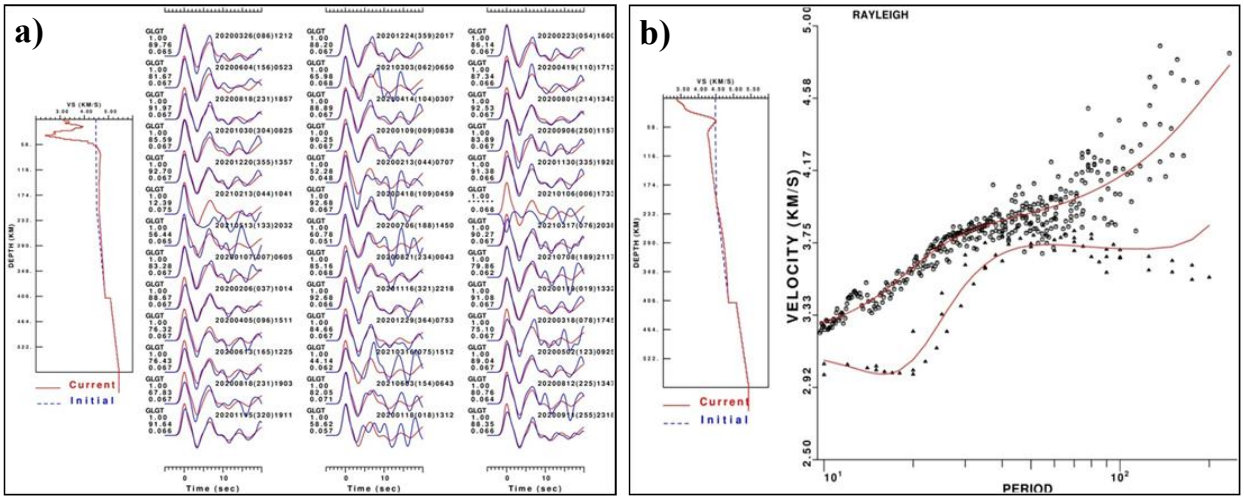

Fig. 9 (a) Inversion Results for GLGT station to obtain earth model using receiver functions inversion. P-wave first arrival times for the true model, solid blue line, and inverted models red. **(b)** Joint surface wave dispersion analysis for GLGT station using receiver functions.

Employing the same dataset as the HK stacking process is shown in Fig. 9 (a), the inversion approach is then used for the receiver functions to determine the S-wave velocity structure. The Modified AK135 model, which is used as the starting model for the inversion, differs from the given model by substituting values obtained at a depth of 50 km. The ones in the upper 50 km, resulted in a constant velocity model up to that depth. Through the use of this strategy, it was ensured that the data closely matched the model, preventing any potential abrupt velocity discontinuities. Although there is a propensity to exaggerate the velocity model in the initial phases of the inversion, no artificial low-velocity area has been purposefully added. In the inversion process, the model is weighted to prioritize the fixation of the deeper structure while allowing significant variations in the upper 50 km. The region between 50 and 100 km receives intermediate weighting. All models exhibit a good fit with their respective data sets, emphasizing the fact that inversions are not unique in our study.

Fig. 9(b) shows joint surface wave dispersion analysis for the GLGT station using receiver functions. The initial and final earth models and dispersion points plotted are in the inversion test. This procedure requires the removal of linear trends from the information, followed by the removal of complex frequency response employing the pole-zero description. A bandpass filter was then employed to the signal, applying frequency limits such as 0.01, 0.02, 0.2, and 0.4 for example, to block extreme intensification of low-frequency and high-frequency noise. It is vital to note the indicated frequency range, between 0.02 and 0.20 Hz, within which the dispersion points can be reliably interpreted.

Source Mechanism of Gilgit Area Earthquake using Yuji Yagi Codes

Yuji Yagi codes (2004) were used to obtain source mechanisms of small to moderate size (Mw 3.5 – 5.3) earthquakes that occurred near Gilgit city using local seismic waveform information documented by the PAKISTAN SEISMIC CENTER seismic network. A magnitude > 3.5 earthquakes are more frequently experienced in Gilgit city. Mainly earthquakes arose in the vicinity of the southwest direction along the MMT fault. Many small earthquake moment tensors are evaluated using GLGT station waveform data. This approach further quantifies their characteristics based on moment tensor inversion results (D'Amico et al., 2011).

The plot labels (Fig.10a-c), on the top left show results of moment tensor evaluation, top match depth, the focuses of the dual nodal level surface, variance and moment magnitude Mw. The Top left beach ball shows twin pair focal procedure; Fault plane solutions from moment tensor analysis of Gilgit area earthquakes Mo [Nm], depth z [km], and the orientation of the two nodal planes.

The determination of moment magnitudes, focal depths, and procedures for earthquakes with magnitudes Mw 4.0 yields satisfactory outcomes. This method is utilized to estimate source parameters using a single seismic station. While the source processes are influenced by the crustal structure, the general faulting pattern (normal, thrust, or strike-slip) remains relatively consistent for the well-constrained solutions presented in Fig.10 (d).

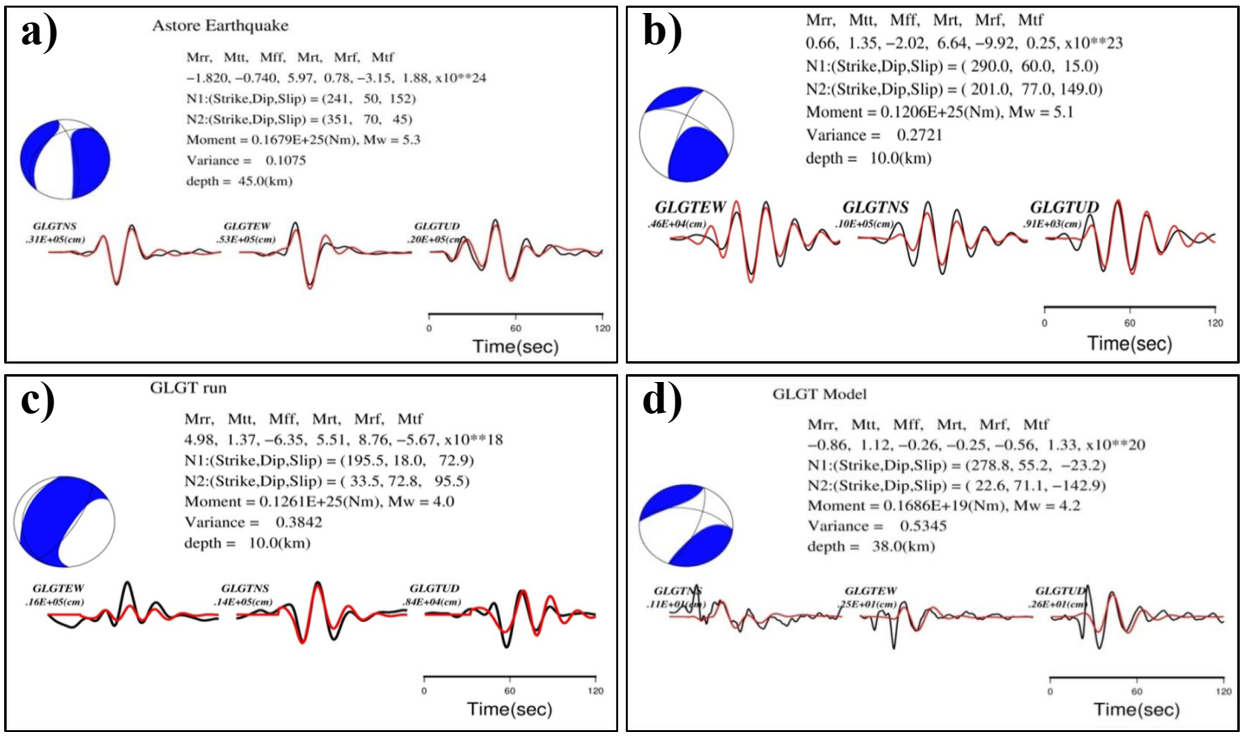

Fig. 10. (a) Moment tensor inversion of Astore earthquake Mw 5.3 occurred on 27th December 2021**. (b)** Moment tensor inversion of Astore earthquake Mw 5.2 occurred on 16th March 2022. **(c)** Moment tensor inversion of Astore earthquake Mw 4.0 occurred on 31st December 2019 about 44 km southeast from GLGT station. **(d)** Moment tensor inversion of Astore earthquake Mw 4.2 occurred on February 5th, 2019 along MMT about 74 km NNW of Gilgit city.

The misfit analysis reveals that the plane dipping to the east is strongly constrained by a dilation on the incorrect side of the nodal plane. On the other hand, the orthogonality criterion provides reasonably good constraints for the other nodal plane. However, the aftershock distribution suggests that the fault plane corresponds to the east-dipping plane, with a depth range of 38 km and a lateral range of approximately 8 km. The strike of this plane is nearly matching to the western boundary of the MMT. The determination of the over-thrust solution is based on the analysis of body wave amplitudes. In some cases, the fault-plane solution for these earthquakes recorded by the PAKISTAN SEISMIC CENTER seismic network was obtained using the first motion of P-waves. Focal mechanisms for earthquakes in Gilgit were determined by analyzing the first motion of P-waves, utilizing a simple crustal velocity model. The focal mechanism of this earthquake verified in current research is reliable with the tectonic setting of the area. The results correspond with the Seismotectonic pattern and inquiry of earthquake focal procedures with the dispersal of seismicity near the Gilgit area, an area between MKT and MMT in North Pakistan (Sunilkumar et al., 2023).

Seismicity Evaluation near Gilgit

The crustal thickness changes across northern Pakistan from 50-73 kilometres in the northern areas and varies to 40-450 km for local and regional events. Most of the earthquakes are near the MMT-Raikot fault area. A new crustal model with a crustal thickness of 63 km was identified in our study. It has been analyzed that, local and regional earthquakes gave enough P and S-wave. The tectonic setting near Gilgit and its surroundings is dominated by the presence of MKT, MMT and MBT along active mountain ranges and the transition to the high deformation zone in the region (Mottram et al., 2014). However, earthquakes in Gilgit frequently occur of moderate sizes mostly occurring in the northwest part of the Hindukush region and the south zone. Most of these earthquakes occur in the north and south direction from Gilgit city indicating that both MMT and MKT faults are associated with deforming and are not stable (Khurram et al., 2022; Rehman et al., 2021).

Results of SELENA Risk Assessment for Gilgit City

Seismic risk assessment for the Gilgit district has been performed using the SELENA seismic risk estimation tool, developed by NORSAR. The study area was divided into 06 different zones and 110 geo units, based on building inventory, population distribution, and local site conditions for Vs_{30} and Seismotectonic settings. The earthquake catalogue from local and international sources is examined carefully both for recent and past seismic activities near Gilgit. The seismic source mechanisms were obtained from the Global CMT catalogue for significant earthquakes (Mw>5.5) near Gilgit city along the MMT fault. Moment magnitude scale (Mw) is considered for all these earthquakes. New shake maps based on different ground

motion attenuation relations were constructed to assess the maximum possible peak ground acceleration (PGA) in Gilgit city. Earthquake of MW 7.0 along MMT, shows that ground motion produced is comparable with damage assessment obtained from seismic risk assessment results.

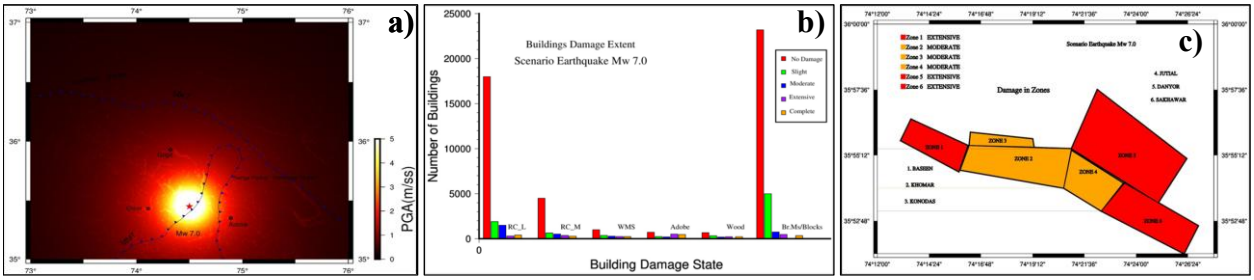

Fig. 11. (a) Geographical distribution of the PGA in m/s^2 using the SIGMA tool and Zao at el. GMPE relation for the scenario earthquake Mw 7.0 PGA **(b)** Building damage state for each building typology for scenario earthquake Mw 7.0 **(c)** Combined damage estimate for each zone for scenario earthquake Mw 7.0.

Similar results were obtained that estimated maximum PGA in the range 0.30 - 0.40 g for northern Pakistan (Molina et al., 2010). The present study aims to estimate seismic risk assessment for Gilgit City, based on updated seismic hazard and ground motion shake maps. These shake maps were calculated using the SIGMA intensity tool and plotted with Generic Mapping Tools. Different ground motion prediction equations were used suitable for local seismotectonic conditions and seismicity of the study area with one earthquake taken as worst case scenario with Mw 7.0 while considering Mw 7.6 Kashmir earthquake in 2005 as a reference (Ali et al., 2009).

Earthquake ground motion information is highly useful in assessing the amount of damage that may have occurred but also helps in understanding the earthquake size of the historical events and the probable loss of life and the built environment. Quantification of earthquake ground motion in terms of the Modified Mercalli Intensity scale (MMI) can also help in assigning various magnitudes to the historic events in any seismogenic area (Table S2 supplementary material). Seismic hazard analysis is among the most common tools to estimate the expected level of intensity of ground motion which is related to seismic events, so it is the fundamental input into the decision-making process for earthquake loss mitigation (Ahmed et al., 2012). These shake maps provide an insight into the question of seismic hazard as well. Therefore, the knowledge of the distribution of the maximum ground values based on reliable methodologies is still a critical issue for the Pakistan region. These values are usually attributed to the presence of partial melt in the mantle wedge and correspond to unusually high melt fractions of the order of 15–20% for a typical mantle composition (Mahéo et al., 2009).

The earthquake along MMT of magnitude Mw 7.0 is considered one of the worst-case scenarios with epicentres located on the MMT close to the Raikot fault at an epicentral distance range about 70 km south of Gilgit is taken to estimate damage and loss using the SELENA risk tool (Molina et al., 2015). The ground motion shake maps were generated using the SIGMA tool and GMT mapping software., The exposure of buildings, selected earthquake scenarios and vulnerability information were provided as input parameters to the SELENA software (Seismic Loss Estimation using a Logic Tree Approach) and were used to obtain potential damage, human and economic loss due to Mw 7.0 earthquake was considered. (Hosseinpour et al., 2021).

The earthquake Mw 7.0 generated maximum damage to the infrastructure with human causalities and injuries in Gilgit city. Ground motion distribution has been estimated based on empirical relation as depicted in Fig. 11 (a). The maximum ground shaking intensity for this earthquake produced in the range VIII-IX at the MMI scale and PGA (Peak Ground Acceleration) is estimated at ~0. 51g. The values show damages that will take place to the structures near the epicentral. The damage estimates shown in Fig. 11 (b) suggest that scenario earthquake with a magnitude of Mw 7.0 occurred at an epicentre approximately 70 km away in the southward direction from Gilgit city along the MMT fault zone posing a very high risk to the Astore most nearby city area along with Chilas. The Earthquake, the building damage state plot shows all types of buildings suffered damage in an earthquake. However, poor brick masonry structures, Adobe and low-rise RF concrete structures suffered more showing RC-L type of buildings may experience higher damage state.

The Fig. 11 (c), presents damaging diverse zones Baseen, Danyor, and Sakhawar, which experienced high level risk in earthquakes having magnitude 7.0. According to Mottram et al., (2014), an earthquake in Gilgit city with a magnitude of Mw 7.0 along the MMT fault zone may pose a very high risk to infrastructure and humans. The building's results estimated as located in the southern part of Gilgit, particularly Gilgit's Southern region is expected to suffer the highest damage as shown in Fig.11 (b). This can be attributed to the proximity of this area to the epicentre of the earthquake and local soil conditions in this area, Zone 01, Zone 05 and Zone 06. On the other hand, the central part of Gilgit city is expected to suffer less damage compared to the Gilgit Southern. This difference can be attributed to the fact that when the focus is on building design and well-constructed infrastructure.

Conclusions

In Gilgit and the adjacent territories, reducing the risk of earthquakes is a big challenge. Seismological data could be very useful to perform the seismic assessment and forthcoming measures to avoid damages in the Gilgit city. A new crustal model for S-wave velocity structure has been generated through waveform inversion. A new crustal model with a crustal thickness of 63 km was successfully identified. The horizontal velocity and phase of a teleseismic subsurface wave (P-wave), which reaches the seismic location, was reasonably stable and high (15–25 km/s). The S-wave velocity was calculated using the one-

dimensional tectonic velocity model and a Vp/Vs ratio of 1.74 was determined. Inversion of P wave radial RF results indicate a shear wave velocity of 3.62 km/s in the crust of Gilgit station located in the Higher Himalayas thrusting region to 4.5km/s underneath the Moho limit. A significant spike in a duration of 7-9 seconds, notably at the GLGT station, was seen with a crustal conversion that happens about 2-3 seconds after the P-arrival. The findings demonstrate that the S-wave velocity underneath northern Pakistan rises between 3.6 km/s to 3.8 km/s. The earthquake along MMT of magnitude Mw 7.0 as one of the worst-case scenarios predicted using the SALENA tool revealed huge damage to infrastructure and causalities in Gilgit City. Hence, it is concluded that to protect people during earth-shaking events, structures must be built by the region's seismic zone. Geological, tectonic, and historical earthquake studies can be used to predict future tremors and create exemplary mitigation plans.

References

1. Ahmed, M., Lodi, S.H., Rafi, M.M., and Alam, N. (2012). Transforming Census Data in Pakistan into Spatial Database for Earthquake Loss Estimation Models. Conference paper: World Conference on Earthquake Engineering at Lisbon, Portugal v.15
2. Ahmed, M.F., Awan, U., and Rogers, J.D. (2021). Use of anomalous topographic features for landslide inventory mapping of Gilgit area, Gilgit-Baltistan, Pakistan. Arabian Journal of Geosciences 14, 1-16.
3. Ahmed, T., Rehman, K., Shafique, M., and Ali, W. (2023). GIS-based earthquake potential analysis in Northwest Himalayan, Pakistan. Environmental Earth Sciences 82(4), 113.
4. Ali, Z., Qaisar, M., Mahmood, T., Shah, M.A., Iqbal, T., Serva, L., Michetti, A.M., and Burton, P.W. (2009). The Muzaffarabad, Pakistan, earthquake of 8 October 2005: surface faulting, environmental effects and macroseismic intensity. Geological Society, London, Special Publications 316(1), 155-172.
5. Ammon, C.J., Randall, G.E., and Zandt, G. (1990). On the nonuniqueness of receiver function inversions. Journal of Geophysical Research. Solid Earth, 95(B10), 15303-15318.
6. Aslam, B., Zafar, A., Qureshi, U.A., and Khalil, U. (2021). Seismic investigation of the northern part of Pakistan using the statistical and neural network algorithms. Environmental Earth Sciences 80, 1-18.
7. Buchan, S.J., Duran, M., Rojas, C., Wuth, J., Mahu, R., Stafford, K.M., et al. (2023). An HMM-DNN-Based System for the Detection and Classification of Low-Frequency Acoustic Signals from Baleen Whales, Earthquakes, and Air Guns off Chile. Remote Sensing 15(10), 2554.
8. D'Amico, S., Orecchio, B., Presti, D., Gervasi, A., Zhu, L., Guerra, I., et al. (2011). Testing the stability of moment tensor solutions for small earthquakes in the Calabro-Peloritan Arc region (southern Italy). Bollettino di Geofisica Teorica ed Applicata.
9. Eulenfeld, T. (2020). Receiver function calculation in seismology. Journal of Open Source Software 5(48), 1808.
10. Goldstein, P., Dodge, D., Firpo, M., Minner, L., Lee, W.H.K., Kanamori, H., et al. (2003). SAC2000: Signal processing and analysis tools for seismologists and engineers. The IASPEI international handbook of earthquake and engineering seismology 81, 1613-1620.
11. Hosseinpour, V., Saeidi, A., Nollet, M.-J., and Nastev, M. (2021). Seismic loss estimation software: A comprehensive review of risk assessment steps, software development and limitations. Engineering Structures 232, 111866.
12. Khalid, P., Bajwa, A.A., Naeem, M., and Din, Z.U. (2016). Seismicity distribution and focal mechanism solution of major earthquakes of northern Pakistan. Acta Geodaetica et Geophysica 51, 347-357.
13. Khurram, S., Khalid, P., Ehsan, M.I., and Muhammad, S. (2022). The seismic hazard and spectral acceleration for hydro power project in Gilgit Baltistan Pakistan. International Journal of Economic and Environmental Geology 13(2), 67-73.
14. Khurram, S., Khalid, P., Qureshi, J., and Din, Z.U. (2021). Assessment of seismic hazard of roller compacted concrete dam site in Gilgit-Baltistan of northern Pakistan. Earthquake Engineering & Engineering Vibration 20(3).
15. Kraft, H.A., Thybo, H., Vinnik, L.P., and Oreshin, S. (2019). Crustal structure in central-eastern Greenland from receiver functions. Journal of Geophysical Research: Solid Earth 124(2), 1653-1670.
16. Li, A., and Mashele, B. (2009). Crustal structure in the Pakistan Himalaya from teleseismic receiver functions. Geochemistry, Geophysics, Geosystems 10(12).
17. Mahéo, G., Blichert-Toft, J., Pin, C., Guillot, S., & Pêcher, A. (2009). Partial melting of mantle and crustal sources beneath South Karakorum, Pakistan: implications for the Miocene geodynamic evolution of the India–Asia convergence zone. Journal of Petrology, 50(3), 427-449.
18. Melouk, B., Yelles-Chaouche, A., Semmane, F., and Galiana-Merino, J.J. (2023). Moho depth variation and shear wave velocity structure in northern Algeria from joint inversion of P-wave receiver functions and Rayleigh wave dispersion data. Geophysical Journal International 233(2), 1229-1244.
19. Molina, S., Lang, D. H., and Meslem, A. (2015). The SELENA–rise open risk package–towards the next generation of ELE software. SECED 2015 conference: earthquake risk and engineering towards a resilient World. 9-10.
20. Molina, S., Lang, D.H., and Lindholm, C.D. (2010). SELENA–An open-source tool for seismic risk and loss assessment using a logic tree computation procedure. Computers & Geosciences 36(3), 257-269.
21. Mottram, C.M., Argles, T.W., Harris, N.B.W., Parrish, R.R., Horstwood, M.S.A., Warren, C.J., et al. (2014). Tectonic interleaving along the Main Central Thrust, Sikkim Himalaya. Journal of the Geological Society 171(2), 255-268.
22. Nemocón, A.M., Julià, J., and Garcia, X. (2021). Lithospheric structure of the western Borborema Province from receiver functions and surface-wave dispersion: implications for basin inversion. Tectonophysics 816, 229024.
23. Poudel, A., Pitilakis, K., Silva, V., and Rao, A. (2023). Infrastructure seismic risk assessment: an overview and integration to contemporary open tool towards global usage. Bulletin of Earthquake Engineering, 1-26.

24. Qadri, S.M.T., Mirza, M.Q., Raja, A., Yaghmaei-Sabegh, S., Hakimi, M.H., Ali, S.H., et al. (2023). Application of Probabilistic Seismic Hazard Assessment to Understand the Earthquake Hazard in Attock City, Pakistan: A Step towards Linking Hazards and Sustainability. Sustainability 15(2), 1023.
25. Qureshi, J.A., Khan, M., Sikandar, S., Khan, G., Abbas, N., Khan, A., et al. (2021). Inventory and Quantitative Valuation of Geological and Geomorphological Sites from Gilgit-Baltistan, Northern Pakistan. Geoheritage 13, 1-15.
26. Rahman, A.U., Najam, F.A., Zaman, S., Rasheed, A., and Rana, I.A. (2021). An updated probabilistic seismic hazard assessment (PSHA) for Pakistan. Bulletin of Earthquake Engineering 19, 1625-1662.
27. Rehman, K., & Burton, P. W. (2020). Seismicity and seismic hazard parameters in and around Pakistan. Journal of Seismology, 24, 635-653.
28. Searle, M.P., and Treloar, P.J. (2019). Introduction to Himalayan tectonics: a modern synthesis. The Geological Society of London.
29. Sunilkumar, T.C., Gahalaut, V.K., Srinagesh, D., and Naresh, B. (2023). Seismotectonic significance of the December 1, 2020 Haridwar, India earthquake (M 4.3), a lower crust event near the Himalayan topographic front. Journal of Earth System Science 132(2), 46.
30. Torsvik, A. (2015). Receiver function analysis-Seismic imaging of the crust beneath TROLL seismic station in Queen Maud Land, Antarctica.
31. Tsapanos, T. M., & Burton, P. W. (1991). Seismic hazard evaluation for specific seismic regions of the world. Tectonophysics, 194(1-2), 153-169.
32. Wang, Q., Niu, F., Gao, Y., and Chen, Y. (2016). Crustal structure and deformation beneath the NE margin of the Tibetan plateau constrained by teleseismic receiver function data. Geophysical Journal International 204(1), 167-179.
33. Waseem, M., Lai, C.G., and Spacone, E. (2018). Seismic hazard assessment of northern Pakistan. Natural Hazards 90, 563-600.
34. Wen, L., Badal, J., and Hu, J. (2019). Anisotropic Hk stacking and (revisited) crustal structure in the southeastern margin of Tibet. Journal of Asian Earth Sciences 169, 93-104.
35. Wessel, P., Smith, W.H.F., Scharroo, R., Luis, J., and Wobbe, F. (2013). Generic mapping tools: improved version released. Eos, Transactions American Geophysical Union 94(45), 409-410.
36. Wilson, J.L., Robinson, A.J., and Balendra, T. (2008). Performance of precast concrete load-bearing panel structures in regions of low to moderate seismicity. Engineering Structures 30(7), 1831-1841.
37. Yagi, Y., Mikumo, T., Pacheco, J., and Reyes, G. (2004). Source rupture process of the Tecomán, Colima, Mexico earthquake of 22 January 2003, determined by joint inversion of teleseismic body-wave and near-source data. Bulletin of the Seismological Society of America 94(5), 1795-1807.
38. Zahoor, F., Ansari, A., Rao, K.S., and Satyam, N. (2023). Seismic Hazard Assessment of Kashmir Region Using Logic Tree Approach: Focus on Sensitivity of PSHA Results Towards Declustering Procedures and GMPEs. Pure and Applied Geophysics 180(3), 789-827.
39. Zandt, G., and Ammon, C.J. (1995). Continental crust composition constrained by measurements of crustal Poisson's ratio. Nature 374(6518), 152-154.
40. Zhang, Y., and Huang, J. (2019). Structure of the sediment and crust in the northeast North China Craton from improved sequential Hk stacking method. Open Geosciences 11(1), 682-696.
41. Zhu, L., and Kanamori, H. (2000). Moho depth variation in southern California from teleseismic receiver functions. Journal of Geophysical Research: Solid Earth 105(B2), 2969-2980.